Journal of the Brazilian Society of Mechanical Sciences and Engineering (2023) 45:94
https://doi.org/10.1007/s40430-022-03874-4

TECHNICAL PAPER

Numerical analysis of lap shear joints made of functionally graded materials

D. Kumar[1] · P. R. Budarapu[1] · A. K. Pradhan[1]

Received: 10 July 2022 / Accepted: 18 October 2022 / Published online: 18 January 2023

Abstract

The strength and life of adhesively bonded joints can be significantly improved by redistributing the stresses at overlap ends over the bond length. One way to achieve this is by varying the material properties, with the help of so-called functionally graded materials (FGM). In this study, stress transfer mechanics in a joint made of a FGM adherend and a homogeneous, isotropic adhesive are investigated. Damage in the adhesive bonded FGM joints manifests as cohesive and adhesive failures. Some of these damages can simultaneously present in the joint. Therefore, the adhesion failure and their propagation in a curved FGM adherend are studied here. All the simulations are performed in a geometric nonlinear finite element (FE) simulation framework using ABAQUS framework. Loss of structural integrity in a lap shear joint made of FGM adherend with a pre-embedded crack at the interface of adherend and adhesive is modelled, and the load transfer and damage propagation are studied. Furthermore, a parametric study of the structural response by varying the parameters: shallowness angle (θ) and compositional gradient exponent (n) are also performed. Based on the results, mode-II is observed to be a dominating mode. The debonding from the substrate is found to initiate from the centre when n is the lowest.

Keywords Strain energy release rate · Functionally graded material · Lap shear joint · Curved adherend · Adhesion failure

1 Introduction

Functionally graded materials are a class of composite materials in which the composition of constituent materials are varied over the domain, in order to achieve desired variation of material properties for specific functional requirement. This is achieved by varying the composition and microstructure of the composites in space following specific laws. Various approaches based on the particulate processing, preform processing, powder metallurgy, centrifugal casting, layer processing and melt processing are used to fabricate the FGMs. On the other hand, dissimilar adherends are also joined through adhesives/bolted joints. In general, joints are the weaker locations leading to concentration of stresses and are prone to damage [1]. The presence of defects in FGM structural member can lead to degradation of their stability and load carrying capacity. Adhesives are strong in shear and weak in resisting peel stresses. Surface condition, fillet geometry [2], adhesive thickness, strength of the adhesive [3], surface ply orientation angle [4], type of loading, geometry and configuration of the joint are some of the parameters causing the adhesion failure.

An analytical model for an adhesively bonded single lap joint with FG adherends and double lap adhesive joints to estimate the critical locations of stress concentration are developed in [5, 6]. The through-the-thickness stress variations of functionally graded plates subjected to thermo-mechanical loads are analysed in [7], based on the third-order shear deformation plate theory. Furthermore, functionally graded adhesive joints made of dissimilar adherends subjected to combined mechanical and thermal loads in a one-dimensional bar was studied in [8]. An analytical model for the stress analysis of functionally graded adhesive single lap joints considering peel and shear stresses in the adhesive, along with the nonlinear geometric characteristics and adhesive Young's modulus variations, is proposed in [9]. On the other hand, a comparative study of the analytical models for planar functionally graded adhesive single lap joints is provided in [10]. A review on the

Technical Editor: João Marciano Laredo dos Reis.

✉ A. K. Pradhan
akpradhan@iitbbs.ac.in

[1] School of Mechanical Sciences, Indian Institute of Technology, Bhubaneswar 752050, India

analysis of bonded joints with FGM adherends using analytical, numerical and experimental methods indicated that several different techniques for obtaining FGMs have been proposed in the literature [11]. Whereas, experimental studies on the practical application of the developed techniques is reported to be limited.

An analytical model for the stress analysis in a tubular single lap joint (SLJ) subjected to torsion with a functionally graded modulus adhesive was developed in [12, 13]. Furthermore, a theoretical framework for the stress analysis of adhesively bonded tubular lap joints consisting of a functionally modulus graded bond-line adhesive by varying modulus of the adhesive along the bond-length is discussed in [14]. A three-dimensional free vibration analysis of an adhesively bonded functionally graded single lap joint made of ceramic and nickel phases varying through the plate thickness is presented in [15]. The rate of propagation of embedded pre-existing delamination in the strap adherend of lap shear joint made of carbon/epoxy composites was evaluated [16] with the help of a three-dimensional nonlinear finite element model. A dynamic instability analysis of fibre-reinforced composite cantilever beams using numerical and experimental studies is performed in [17]. Low-velocity impact analysis of glass fibre-reinforced polymer (GFRP) and hybrid laminates is performed in [18, 19] through an explicit numerical analysis and relevant experiments.

The fatigue behaviour of hybrid bolted-bonded single-lap shear joints made of carbon fibre-reinforced composites was investigated in [20]. The stress transfer mechanics and hence the failure mechanisms in nacre-like brick-mortar structures was investigated in [21, 22], thereby, a framework to design nacre-inspired composites incorporating a functionally modulus graded interphase material was proposed. A non-intrusive approach coupled with non-uniform rational B-splines-based isogeometric finite element method for the analysis of functionally graded plates with material uncertainty is proposed in [23] Moreover, a methodology based on the shear-lag theory to study the mechanics of stress transfer in a three-phase composite system considering both homogeneous and inhomogeneous interphases in a curved-fibre pull-out test is introduced in [24]. The intra- and inter-layer bridging mechanisms in matrix/fibre composites through crack simulation coupling the phase field approach and the cohesive zone model is introduced in [25], to identify crack migration through material layers. Inter-laminar stresses in the adhesive layer between the lap and the strap adherends of lap shear joints made of curved laminated fibre-reinforced plastic composite panels were studied in [26, 27].

The main objectives of this study are: (i) To perform three-dimensional adhesion failure analysis of lap shear joints made of curved adherends subjected to axial loads, considering the lap and strap adherends made of functionally graded materials. (ii) Study the influence of parameters shallowness angle (θ) and compositional gradient exponent (n) on the interfacial stresses and strain energy release rate in lap shear joints. All the simulations in this study are performed using the nonlinear commercial finite element (FE) code ABAQUS. The developed numerical framework is validated by comparing the results from the numerical analysis using conventional shell elements S4RS with the results from axi-symmetric analytical solution developed in [14]. Details of the analysis are mentioned in Sect. Appendix A.

The rest of the paper is organized as follows: Sect. 2 presents the modelling aspects of the lap shear joints considering its geometry, variation of material properties and finite element analysis. Analysis of lap shear joint subjected to compressive loads highlighting the variation of peel and shear stresses, and the influence of shallowness angle were discussed in results and discussion Sect. 3.1. Analysis of lap shear joints with a pre-embedded circular debonding region was investigated in Sect. 3.1.2. Key results are summarized in Sect. 4.

2 Modelling aspects

Damage in adhesive bonded joints could be initiated in the adhesive layer, adherends and at the interfaces, depending on the joint configuration, materials, loading, constraints, and the manufacturing procedures. Therefore, it is quite complex to describe all possible modes of damage in adhesive bonded joints. Adhesive bonded lap shear joints are prone to damage during their service, mainly because of high gradients of peel and shear stresses at the overlap ends. In this study, pre-existing failure at the interface of the adhesive and a strap adherend is assumed and debonding the two parts of the specimen at the surface of contact are modelled. However, the strength and service life of the adhesive bonded lap shear joint [28] can be improved by redistribution of the peek interfacial stresses in the vicinity of the adhesion failure front with suitable gradation of material properties of the adherends. This is achieved by varying the material properties, with the help of so-called functionally graded materials. Hence, the lap and strap adherend panels are assumed to be made of FGM. The usage of FGM adherends in the LSJ with suitable gradation of Young's modulus and Poisson's ratio along the length of adherends, in particular, at the critical region of the joint is a technique to reduce the magnitude of interfacial stresses in the vicinity of the adhesion failure front. Thus, the adhesion failure propagation can be delayed with the help of functionally graded adherends.

An attempt is made here to design adhesive bonded lap shear joints for safe carrying loads. Therefore, a three-dimensional nonlinear finite element analysis of the proposed LSJ made of curved FGM adherend panels is performed to identify the maximum load carrying capacity

before failure. The lap and strap adherends composed of ceramic (aluminium oxide, Al_2O_3) and metal (Nickel, Ni), respectively, are joined by an isotropic adhesive material. The material properties of the adherends are graded by varying the composition of constituents, shape, and size [29].

The geometry, loading, and boundary conditions of the proposed lap shear joint made of FGM curved panels are shown in Fig. 1. A schematic of clamped curved lap shear joint with graded lap and strap adherends joined by an adhesive is shown in Fig. 1a, where the sectional view at X-X is provided in Fig. 2a. The metal, adhesive and ceramic parts around the free end of the lap adherend are highlighted in a close-up of Fig. 2a. A discretized model of a part of the lap shear joint around the free end of lap adherend is shown in Fig. 1b. Three-dimensional hexahedral elements, i.e. C3D8S and C3D8R elements available in ABAQUS, are used for the discretization. The selected elements support full as well as reduced integration schemes, which is essential to perform the geometric nonlinear analysis of curved shear lap joints.

The thickness of the lap and strap adherends and adhesive are adopted as 1 mm each and 0.2 mm, respectively, see the close-up of Fig. 2a. The lengths of lap and strap adherends are adopted as 45 and 125 mm, respectively. The inner radius of strap adherend is adopted as 71.6 mm and the shallowness angle (θ) is considered to be 20°. The Young's modulus and Poisson's ratios of constituents of lap shear joints are listed in Table 1.

One end of the LSJ is clamped and the free end is loaded with a displacement of 0.1 mm along the axial direction, see Fig. 2a. The contact between the adherend and adhesive are modelled as slave and master surfaces. Furthermore, in order to ensure the computational efficiency as well as accuracy, the mesh is adaptively generated such that fine grading is ensured around the free end of the lap adherend, as shown in Fig. 1b. However, the element size in the simulations is selected after a through convergence study. Convergence is observed when the total number of elements is ≈141584 elements. Accordingly, the number of elements used in all the simulations is equal to 141584 which corresponds to a total number of 191394 nodes. Furthermore, 118724 number of linear hexahedral elements of type C3D8S and 22860 number of linear hexahedral elements of type C3D8R are used to discretize the adherend and adhesive, respectively. The strain energy release rate (SERR) is computationally estimated using virtual crack closure technique (VCCT) in ABAQUS, satisfying the requirements, like: symmetric mesh on the damage plane, small element size and maintaining the regular finite element mesh around the damage front.

In the present study, the elastic modulus and the Poisson's ratio of the lap and strap FGM are varied along the axial direction according to a polynomial law with an exponent (n), as mentioned below:

$$E(z) = \begin{cases} E_m + (E_c - E_m)\left(\frac{x}{l_1}\right)^n & \text{if} \quad 0 \le x < l_1 \\ E_m + (E_c - E_m)\left(\frac{x-l_1}{l-l_1}\right)^n & \text{if} \quad l_1 \le x \le l \end{cases} \tag{1}$$

$$\nu(z) = \begin{cases} \nu_m + (\nu_c - \nu_m)\left(\frac{x}{l_1}\right)^n & \text{if} \quad 0 \le x < l_1 \\ \nu_m + (\nu_c - \nu_m)\left(\frac{x-l_1}{l-l_1}\right)^n & \text{if} \quad l_1 \le x \le l \end{cases} \tag{2}$$

where x indicates the axial coordinate, l and l_1 are the lengths of strap and lap adherends, respectively, see Figs. 1a and 2a. E_m, ν_m, and E_c, ν_c are the Young's modulus and Poisson's

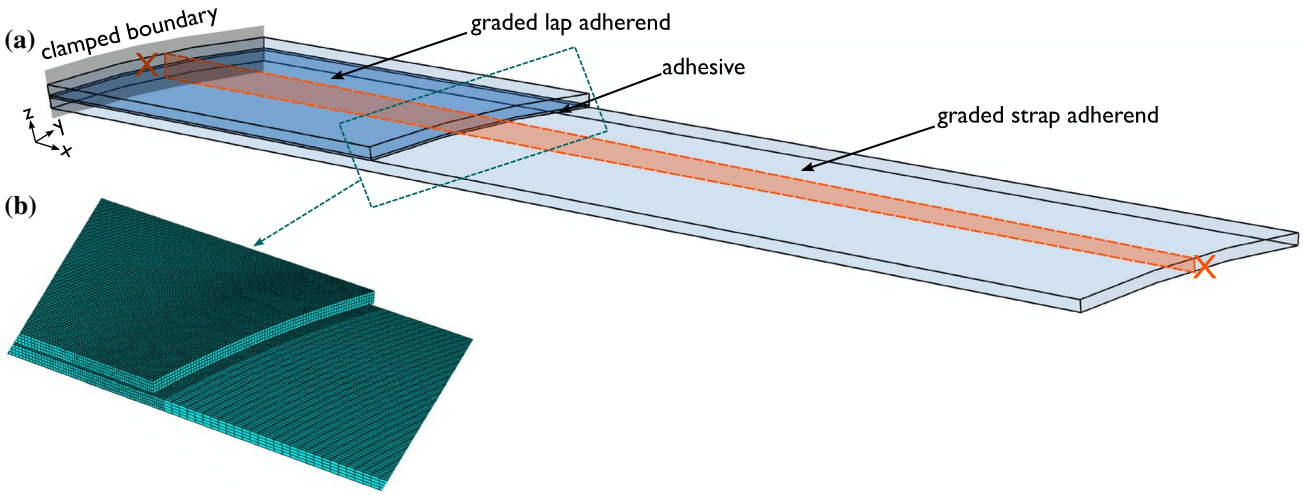

Fig. 1 **a** Schematic of a clamped curved shear lap joint with graded lap and strap adherends joined by an adhesive. Sectional view at X-X is provided in Fig. 2a. **b**. Discretization of a part of the lap shear joint around the free end of lap adherend

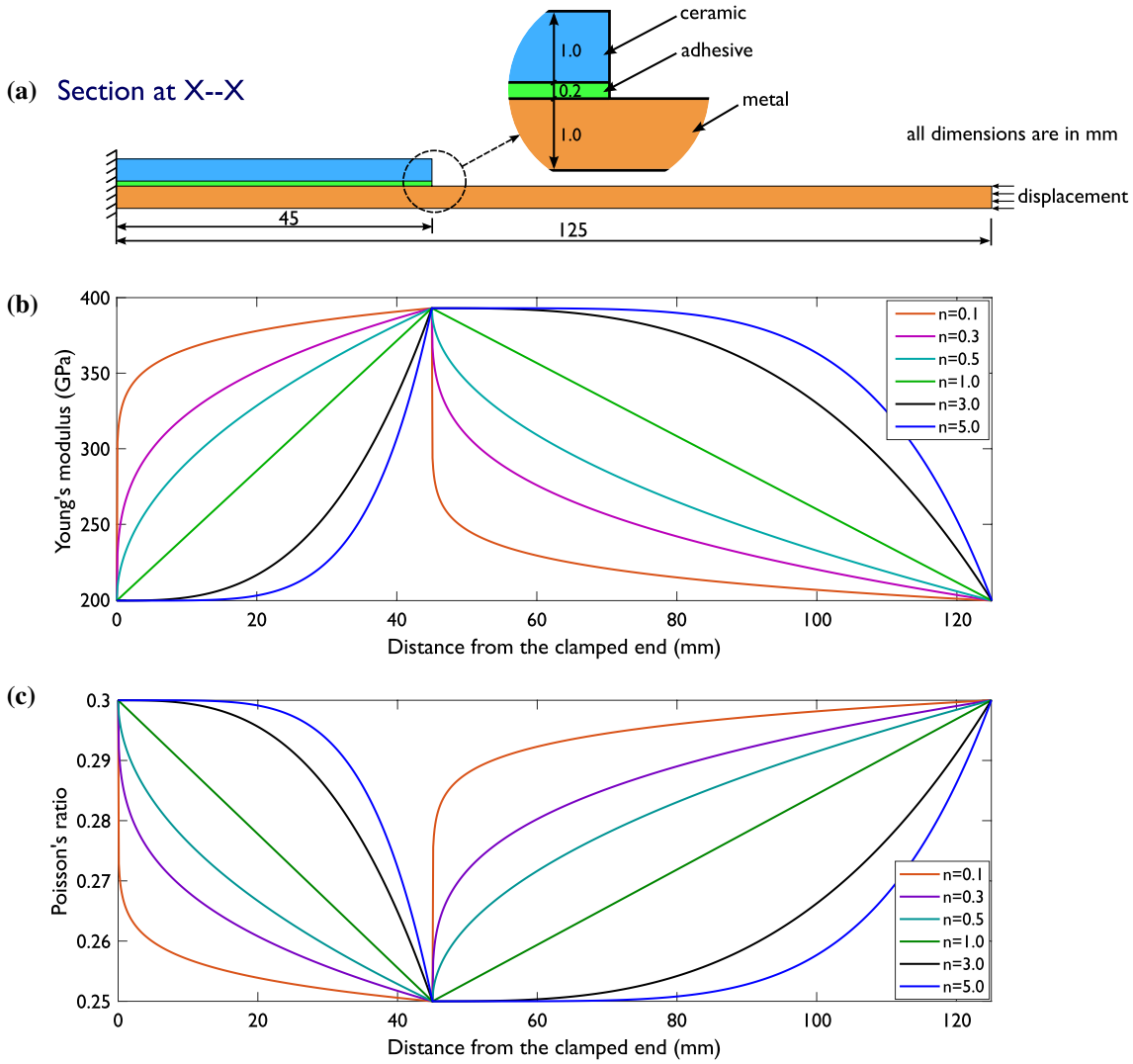

Fig. 2 **a** Sectional view at X-X of the lap shear joint in Fig. 1a. The metal, adhesive and ceramic parts around the free end of the lap adherend are highlighted in a close-up. Variation of the **b** elastic modulus and **c** Poisson's ratio along the length of the shear lap joint according to polynomial laws in Eqs. (1) and (2), respectively

Table 1 The Young's modulus and Poisson's ratios of constituent materials of lap shear joints, adopted from [29]

Constituent	Young's modulus (GPa)	Poisson's ratio
Metal	199.5	0.30
Adhesive	2.4	0.32
Ceramic	393.0	0.25

ratios of pure metallic and ceramic parts, respectively. Variation of the Young's modulus and Poisson's ratio according to Eqs. (1) and (2) is plotted in Fig. 2b and c, respectively. According to Fig. 2b, the modulus is varied in the range of 200–400 GPa, where the modulus is maintained minimum at clamped end and the loaded end of the strap adherend and maximum at the overlap region. This ensures the stiff lap adherend at the joint, thus, the chances of damage initiation will be significantly reduced. Furthermore, the elastic modulus is found to be exhibiting a decreasing trend with increase in grading exponent (n) within the range $0 \leq x < l_1$. Whereas, a reverse trend is observed in the range $l_1 \leq x \leq l$. On the other hand, based on Fig. 2c, the Poisson's ratio is varied in the range of 0.25−0.3, where it is prescribed maximum at clamped end as well as at the loaded end of the strap adherend and minimum at the overlap region. However, the Poisson's ratio is found to be following an increasing trend with increase in grading exponent (n) within the range $0 \leq x < l_1$. Whereas, a reverse trend is observed in the range $l_1 \leq x \leq l$. The varying properties of FGM are realized by

adjusting the proportions of metal and ceramic portions in the composite.

3 Results and discussion

3.1 Lap shear joint subjected to compressive loads

Three-dimensional FE analyses are performed on the developed lap shear joint to estimate the stress field in the domain. Displacements loads of 0.1 mm per step are specified on the tip surface of the strap adherend until the damage initiation at the joint. The location of the adhesion failure in the LSJ can be identified based on the stress distribution. All the six components of stresses on the vulnerable surfaces, i.e.: the bond line interface of the lap adherend and the adhesive and the interface of the strap adherend and the adhesive, are captured to identify the potential locations of failure initiation.

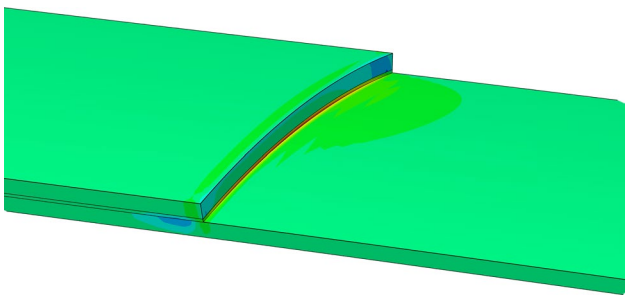

Fig. 3 Three-dimensional distribution of peel stresses in the overlap region of the LSJ. The stress at the lap and adhesive interface end are estimated to be 17 MPa and at the end of strap and adhesive interference is found to be 25 MPa, see Fig. 4b

Three-dimensional peel stress distribution in the overlap region of the LSJ is shown in Fig. 3.

3.1.1 Variation of peel and shear stresses, and SERR with debond length

Distribution of the peel stresses in the overlap region and along the circumference at the joint location are plotted in Fig. 4a and b, respectively.

A zero overlap length indicates the joint location, i.e. $l = l_1$. Whereas, overlap length equal 45 mm denotes the clamped boundary. As shown in Fig. 4a, the peel stresses are observed to be maximum at the overlap ends, followed by a drastic reduction within a small distance from the joint location and almost constant amplitude over the rest of the domain length. The variation of peel stresses along the circumference of the FGM is plotted in Fig. 4b. As shown in Fig. 4b, the peel stresses are maximum along the centre line of the adherend ($\theta = 0^\circ$) and minimum towards the edges. The peel stresses are primarily responsible for the damage initiation. Whereas, the amplitude of shear stress denote the tensile load carrying requirements. The shear stresses in the LSJ are noticed to abruptly change around the overlap region. The non-uniformities in the peel and shear stress distributions are because of the presence of free edge. On the other hand, the peel and shear stresses are observed to be the highest in the overlap region, leading to concentration of stresses. Therefore, based on the stress distribution at the interface shown in Fig. 4, the adhesive and the strap adherend interface at the overlap end is prone to adhesion failure. Therefore, adhesion failure propagation is analysed considering different initial lengths of pre-embedded adhesion damage.

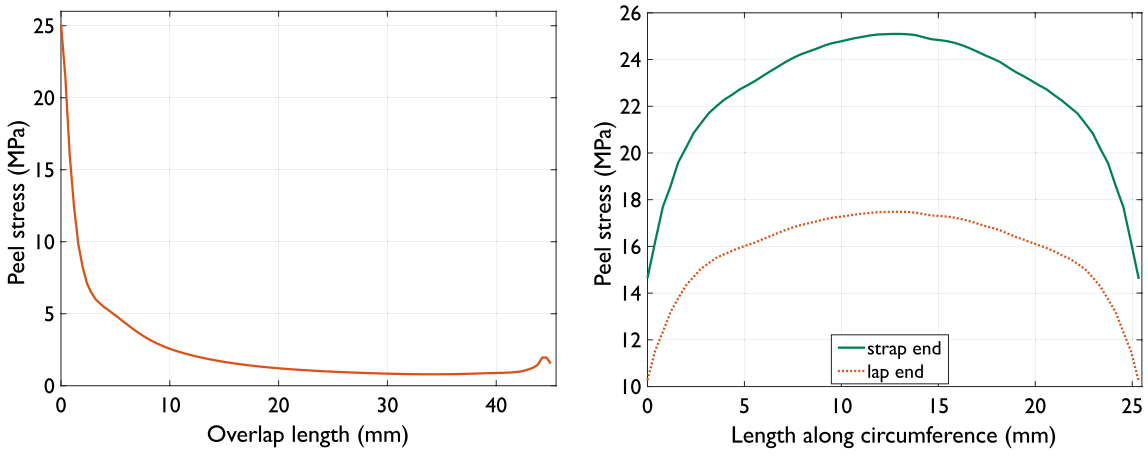

Fig. 4 Distribution of the peel stresses **a** in the overlap region and **b** along the circumference. A zero overlap length indicates the joint location, i.e. $l = l_1$. Whereas, overlap length equal 45 mm denotes the clamped boundary, see Fig. 2a

The influence of grading exponent (n) indicating the composition of FGM on the interfacial stresses in the vicinity of failure front at the interface of adhesive and the curved FGM strap adherend of the LSJ are shown in Fig. 5a and b. The variation of peel and shear stresses with respect to the debond length considering grading exponent values in the range of 0.1 to 10 is shown in Fig. 5a and b, respectively.

Based on Fig. 5a, the peel stress is observed to be initially increasing with increase in debond length until 5 mm, followed by a decrease. This is due to the fact that large stresses are required to separate the adherends from the adhesive when the damage size is small. The strength of the joint reduces with increase in damage size, leading to lower peel stresses at higher debond lengths. Therefore, a drop in peel stresses is evident for debond lengths beyond 5 mm. Furthermore, the peel stress is found to be increasing with increase in grading exponent. This is because the elastic modulus is decreasing with increasing n. Therefore, the stiffness of the structure decreases with increasing n.

The longitudinal shear stresses are noticed to be increasing with the increase in adhesion damage until 3 mm. This is followed by a decreasing trend till the damage size equal to 7 mm. Moreover, the rate of decrease is found to be steep when the debond length is more than 5 mm. Therefore, the shear stresses also observed to be following similar trend as that of peel stresses. However, the decreasing trend starts early at debond length equal to 3 mm. In the similar lines, the shear stresses are also found to be increasing with increase in grading exponent. The maximum values of the peel and shear stresses are observed around the centre region, i.e. at θ equal to 0°, see Fig. 4b.

The strain energy release rate (SERR) in the first, second, third modes and the total SERR in all the modes are plotted with respect to the debond length in Fig. 5c, d, e and (f), respectively, considering different gradient exponent values. According to Fig. 5c, the SERR in mode-I (G_I) is observed to be initially decreasing with increase in adhesion failure size from 1 to 3 mm, followed by an increase. The trend is opposite to the variation of peel stress in Fig. 5a. The SERR in mode-II (G_{II}), plotted in Fig. 5d is found to increase with the increase of the adhesion failure length up to 5 mm. Whereas, it is increasing with the increase in compositional exponent gradient (n). In other words, the magnitudes are lower for lower values of n. The maximum values of G_I and G_{II} are observed at the centre, i.e. at θ equal to 0°. The SERR in mode-III (G_{III}) is plotted in Fig. 5e, where the maximum G_{III} values are observed at the edges. To summarise, G_{II} is estimated to be the dominating mode of failure. The total strain energy release rate in all the modes plotted in Fig. 5f is observed to increase for debonds lengths equal to 1 to 3 mm except for when n equal to 0.1. Therefore, n equal to 0.1 is the ideal selection for grading the material property.

3.1.2 Influence of shallowness angle

The influence of shallowness angle on the crack growth is studied by considering its variation within 20°, after adopting n equal to 0.1. Variation of the strain energy release rate in modes I, II, III and the sum of all the three modes with respect to the distance along the circumference for shallowness angles equal to 0, 5, 10, 15 and 20° are plotted in Fig. 6a, b, c and d, respectively.

The SERR in mode-I when θ varies from 0 to 20° is plotted in Fig. 6a. According to Fig. 6a, the maximum values of SERR is observed around the mid point of the circumference, i.e. when θ equal to 0° and continue to decrease with increase in θ. Therefore, the minimum of the maximum SERR is noticed when θ equal to 20°. Furthermore, the SERR in mode-II when θ varies from 0 to 20° is plotted in Fig. 6b. Based on Fig. 6b, the SERR is observed to be maximum when θ equal to 20° and minimum when θ equal to 0∘, occurring at the midpoint of circumference. The behaviour in mode-II is observed to be opposite to the trend in mode-I. On the other hand, the SERR for mode-III when θ varies from 0° to 20° is plotted in Fig. 6c, where the SERR is estimated to be maximum around the edges and minimum at the centre. The total SERR is plotted in Fig. 6d and noticed that it is dominated by mode-II. Therefore, the total SERR is maximum when θ equal to 20° and minimum for θ equal to 0°, occurring at the middle of the circumference.

To summarise, mode-II is observed to be the dominating mode and SERR is the highest when θ equal to 20°. The maximum value of SERR in mode-II occurs at the centre of the pre-embedded failure. Therefore, the structure in such a loading will be more unstable as compared to the other configurations. Loading in mixed mode indicated that the maximum value of the total SERR occurs at the centre when θ equal to 20°. Therefore, the structure will always open up from the centre. The curvature of the panel influences the debonding propagation resistance, where flat structure are better in resisting the debonding. In other words, as the curvature increases the maximum of the SERR also increases.

3.2 Analysis of LSJ with a pre-embedded circular debonding region

A lap shear joint with a pre-embedded circular debonding region considering the same loading, geometry and boundary conditions as discussed in Sect. 3.1 is considered. Circular debonding region of radii 2, 3 and 4 mm are pre-induced at the interface of the adhesive and the strap adhered, as shown in Fig. 7a. The material properties of the adhesive as well as the functional grading of adherend is adopted same as that of the lap shear joint in Sect. 3.1. The centre of circular debond region is located at 7 mm from the overlap end.

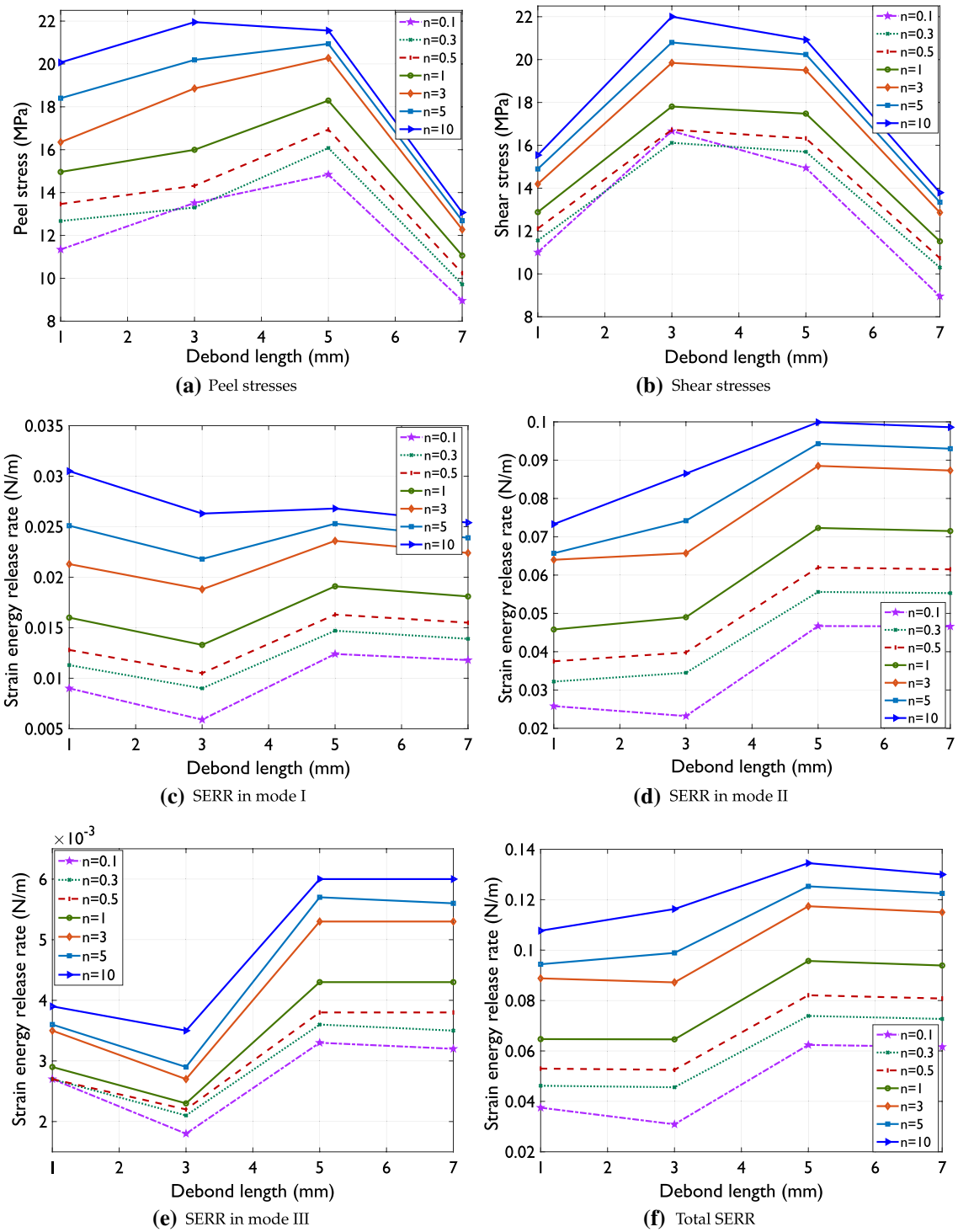

Fig. 5 Variation of the **a** peel and **b** shear stresses with respect to the debond length and grading exponent. Distribution of the strain energy release rate in the **c** first, **d** second, **e** third modes and **f** the total strain energy release rate in all the modes with respect to the debond length

A three-dimensional solid deformable geometry is created for both adherend as well as adhesive separately in part module of ABAQUS, followed by assembly in the assembly module. The joint is discretised using 8-node C3D8S linear brick elements, where the discretisation is adaptively refined as shown in Fig. 7b. The material properties are assigned to the constituents in the property module. The varying material properties for the adherend with temperature are

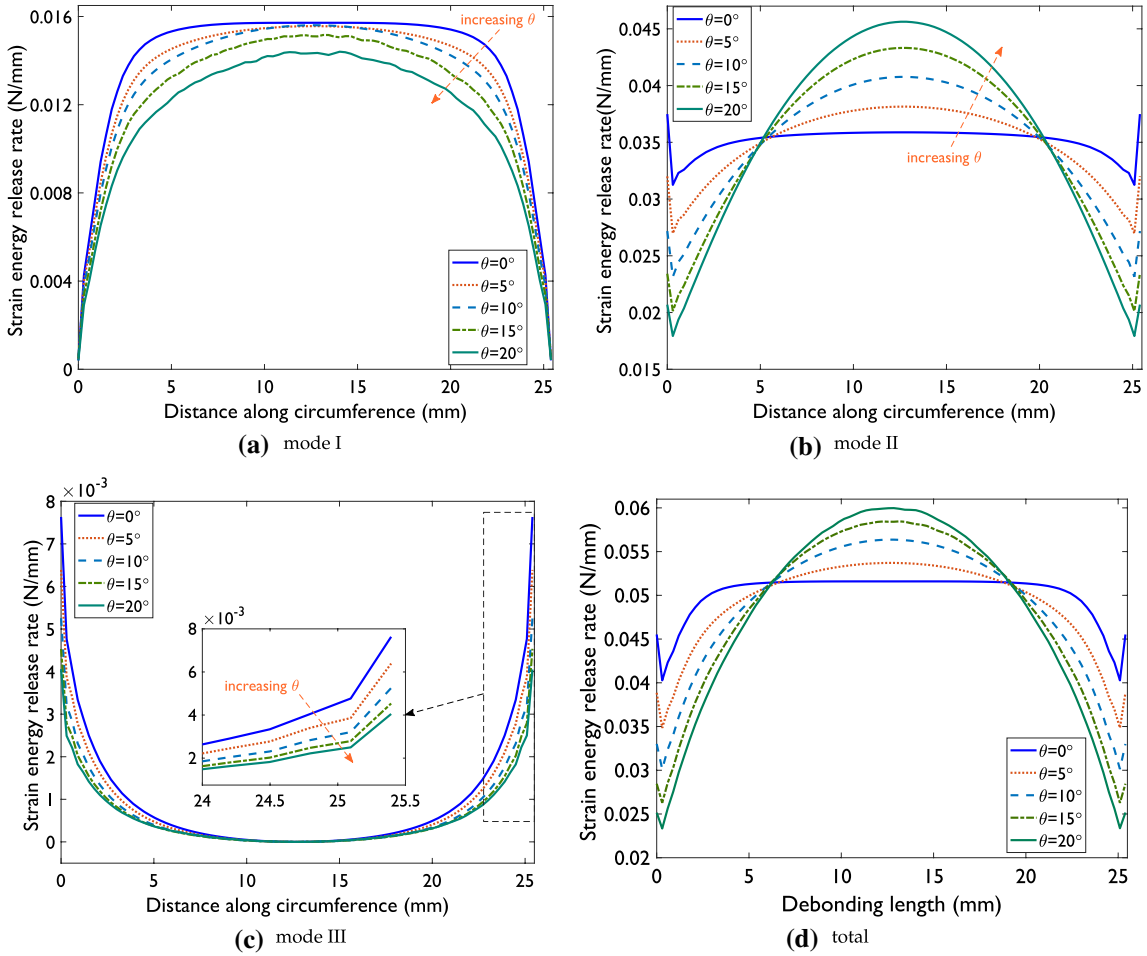

Fig. 6 Variation of the strain energy release rate in the **a** first, **b** second, **c** third modes and **d** the total strain energy release rate in all the modes with respect to the distance along the circumference for shallowness angles equal to 0, 5, 10, 15 and 20°

considered in the analysis with zero coefficient of thermal expansion. The contact between the adherend and adhesive are modelled as slave and master surfaces. Pre-induced crack surfaces are assumed to be partially bonded initially such that the crack tips can be explicitly identified in ABAQUS. The pre-embedded crack is modelled by debonding the contact surfaces. In other words, a nodal set is defined in front of the crack tip along the direction of crack growth, and the corresponding edge nodes are debonded.

The strain energy release rates in three modes, G_I, G_{II} and G_{III} are evaluated using the virtual crack closure technique (VCCT). The fracture behaviour and progressive growth of embedded circular delamination in the LSJ is characterised based on the SERR. The variation of SERR in modes I, II and III (G_I, G_{II} and G_{III}) around the pre-embedded circular delamination of radii equal to 2, 3, and 4 mm at the interface of the adhesive and the strap adherends of the LSJ made of flat FGMs panels are shown in Fig. 8.

The amplitude of SERR in mode I (G_I) around the circular debond region is found to be of the order 10^{-8}, which is significantly smaller as compared to the SERR in modes II (G_{II}) and III ($G_{|||}$), which range in the order of 10^{-3} and 10^{-4}, respectively, see Fig. 8. Therefore, the distribution of SERR is not shown. Furthermore, the SERR is found to increase with increase in radius of the circular debond region in all the modes, see Fig. 8. This is because as the radius of the pre-embedded circular delamination region increases, the size of void at the interface increases, which leads to the reduction structural integrity and strength thereby accelerating the debonding. According to Fig. 8a and c, the SERR in mode II and total SERR exhibits similar pattern, since mode II is the dominating mode. Moreover, as shown in Fig. 8b, in mode III the SERR peaks are observed at angle of 50°, whereas, the corresponding peak is observed at 0° in mode II, see Fig. 8(a-b). Furthermore, the distribution of SERR in Fig. 8 is observed to be symmetric, due to the symmetry in material properties, loading and boundary conditions around circular debond region.

Furthermore, two lap shear joints identical in geometry, loading and boundary conditions, joined by different

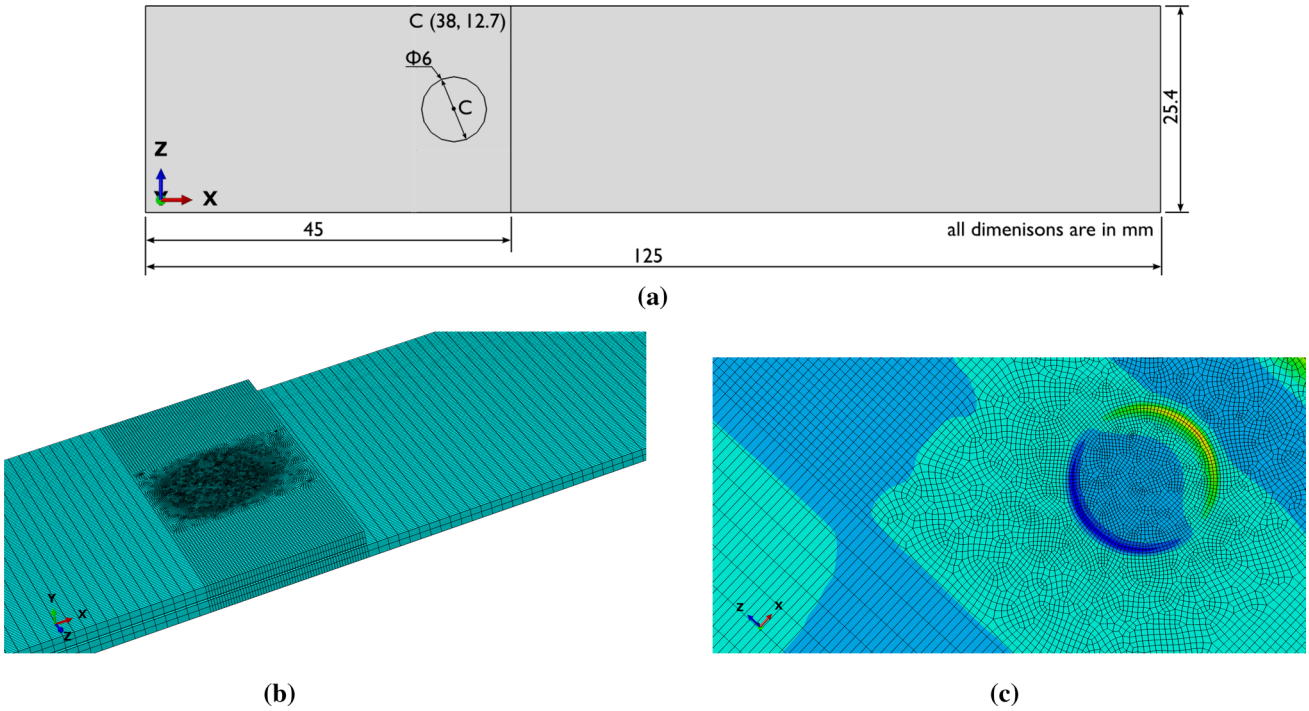

Fig. 7 **a** Schematic of the lap joint with a pre-embedded circular debonding region. **b** Refined adaptive discretisation and **c** the distribution of the peel stresses around the circular debonding region, highlighting the location prone to adhesion failure

adherends made of (i) FGM and (ii) Gr/E laminated unidirectional composite (FRPC) are studied to estimate the adhesion failure, considering pre-embedded adhesion failure of sizes 1 and 3 mm at the interface of isotropic adhesive and strap adherend. Distribution of the SERR with the distance along the circumference for modes I and II is plotted in Fig. 9a and b, respectively. According to Fig. 9, the SERR for both the modes of LSJ with FGM adherend is observed to be lower than the LSJ with FRPC adherend. Therefore, the LSJ made of FGM adherend is more stable as compared to the LSJ made of FRPC adherends. On the other hand, the SERR is found to decrease with increase in pre-embedded adhesion failure of size.

4 Conclusions

The peak stresses in adhesively bonded joints can be reduced by redistributing them over the bond length. In this study, this is achieved by varying the material properties, with the help of so-called functionally graded materials (FGM). Curved lap shear joints are considered for the analysis, where the peel stresses are found to be much higher at the overlap end and drastically drops down with a small distance to remain approximately constant throughout the overlap length. Furthermore, due to such a variation in peel stress the SERR in all modes is found to be the lowest when the compositional gradient index (n) is equal to 0.1. This is also results in the lowest peel stress, which further helps in arresting the adhesion failure.

The variation of SERR for panels with different shallowness angle varying from 0 to 20° is also investigated and observed that the flat panel with θ equal to 0° results in lowest value of SERR. Thus, flat structures are better in arresting growth of adhesion failure as compared to the curved structures. Furthermore, the growth of circular pre-embedded adhesion failure is studied and the variation of SERR around the circumference indicated that the location of damage growth is close to free edge.

A comparison of the FRC and FGM panels with similar geometry and boundary conditions indicated that the panel made of FGM yielded the lowest SERR. Therefore, the use of FGM structures enhance the life of adhesively bonded structure.

Appendix 1: Validation of the finite element framework

Axisymmetric analytical solution developed in [14] is used to validate the developed numerical framework in this study. Therefore, geometric linear analysis was performed using conventional shell elements S4RS. The geometry, boundary conditions, tube material, and loading conditions are

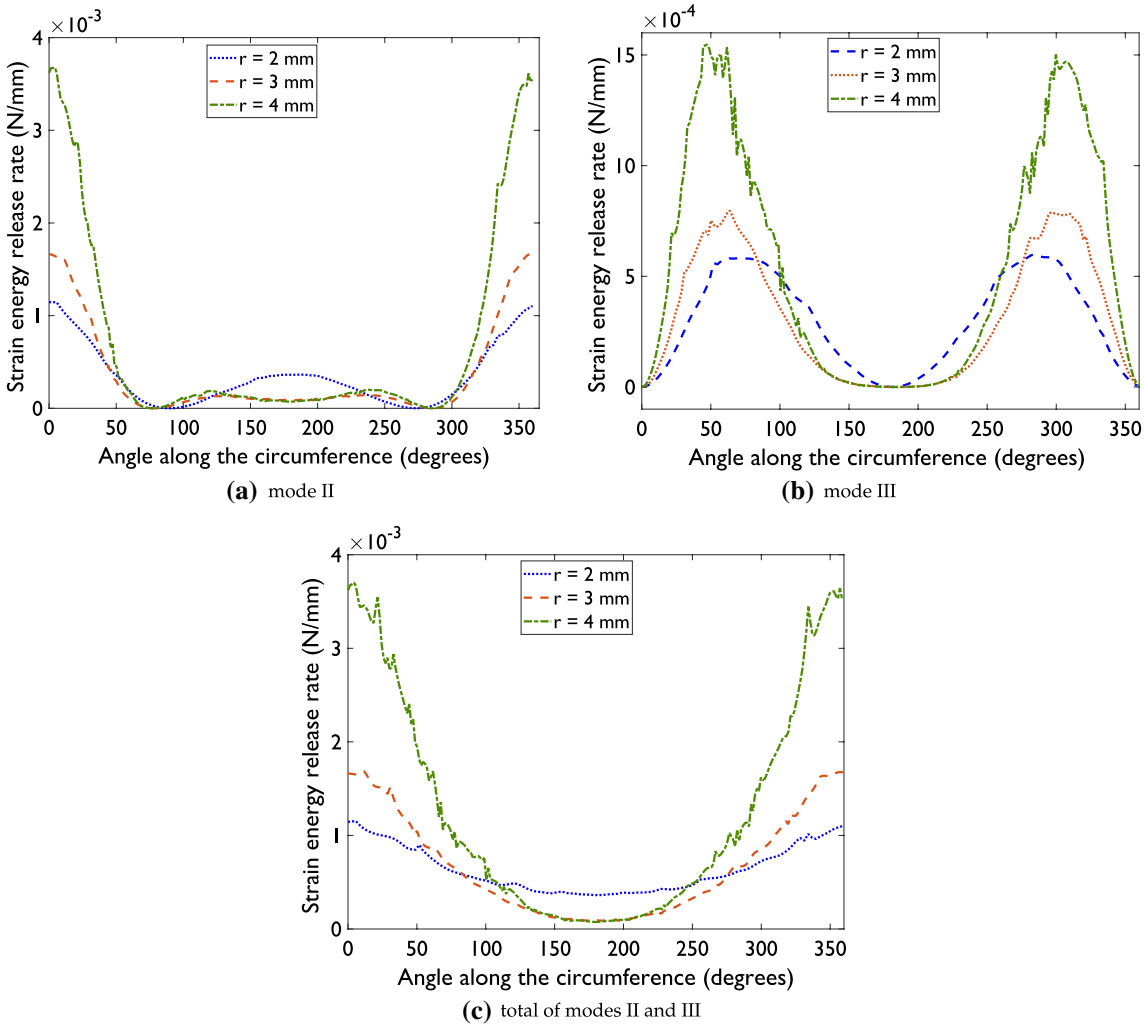

Fig. 8 Variation of SERR in **a** mode II, **b** mode III and **c** the total of modes II and III, near the pre-embedded circular delamination

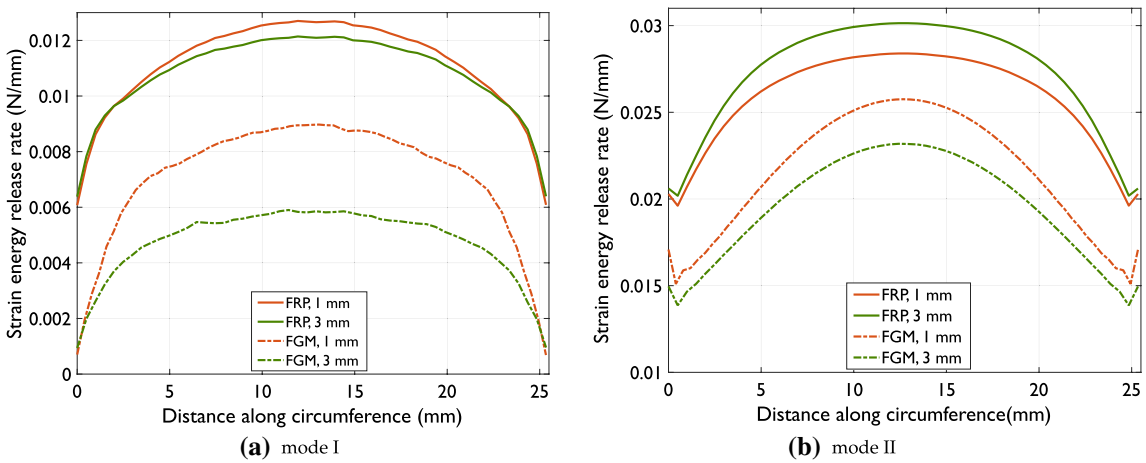

Fig. 9 Distribution of the SERR with the distance along the circumference for modes **a** I and **b** II

adopted from reference [14]. Figure 10 shows a comparison of the peel stress distribution obtained through present numerical solution with the published results in [14]. The maximum error between the present and published results is found to be 0.113%.

Acknowledgements The second author (PRB) is thankful to the Science and Engineering Research Board, Department of Science and Technology, India, for funding this research through grant number SRG/2019/001581.

Data Availability The raw/processed data required to reproduce these findings cannot be shared at this time as the data also forms part of an ongoing study.

Declarations

Conflict of interest The authors have no conflict of interest to declare.

References

1. Agarwal R, Gupta V, Singh J (2022) Additive manufacturing-based design approaches and challenges for orthopaedic bone screws: a state-of-the-art review. J Braz Soc Mech Sci Eng 44(1):1–25
2. Adin H (2017) Effect of overlap length and scarf angle on the mechanical properties of different adhesive joints subjected to tensile loads. Materials Testing 59(6):536–546
3. Wei X, Shen H-S, Wang H (2022) Effect of interfacial energy combined with geometrical nonlinearity on the finite fracture analysis of composite single-lap joints. Compos Struct 280:114938
4. Sadeghi A, Mahshid R, Heidari-Rarani M, Lessard L (2022) Effect of lamina fiber orientation interfaced with semi-flexible adhesive layer on strength and failure mode of composite single-lap joints. Int J Adhes Adhes 118:103232

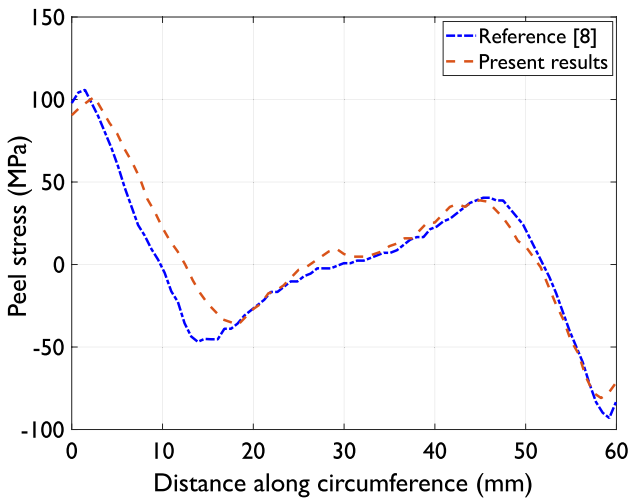

Fig. 10 Comparison of peel stresses estimated based on the present work with the results published in [14]

5. Guin WE, Wang J (2016) Theoretical model of adhesively bonded single lap joints with functionally graded adherends. Eng Struct 124:316–332
6. Gonçalves DC, Sánchez-Arce IJ, Ramalho LDC, Campilho RDSG, Belinha J (2022) Introductory application of a natural neighbour meshless elastic formulation to double-lap adhesive joints. J Braz Soc Mech Sci Eng 44(2):1–16
7. Reddy JN (2000) Analysis of functionally graded plates. Int J Numer Meth Eng 47(1–3):663–684
8. Paroissien E, da Silva LFM, Lachaud F (2018) Simplified stress analysis of functionally graded single-lap joints subjected to combined thermal and mechanical loads. Compos Struct 203:85–100
9. Stein N, Mardani H, Becker W (2016) An efficient analysis model for functionally graded adhesive single lap joints. Int J Adhes Adhes 70:117–125
10. Stein N, Felger J, Becker W (2017) Analytical models for functionally graded adhesive single lap joints: a comparative study. Int J Adhes Adhes 76:70–82
11. Dos Reis MQ, Marques EAS, Carbas RJC, Da Silva LFM (2020) Functionally graded adherends in adhesive joints: an overview. J Adv Join Process 2:100033
12. Spaggiari A, Dragoni E (2014) Regularization of torsional stresses in tubular lap bonded joints by means of functionally graded adhesives. Int J Adhes Adhes 53:23–28
13. Rudawska A, Wahab MA, Müller M, Stančeková D (2022) Mechanical properties and leak-tightness of polymeric pipe adhesive joints. Applied Mechanics 3(1):64–77
14. Kumar S (2009) Analysis of tubular adhesive joints with a functionally modulus graded bondline subjected to axial loads. Int J Adhes Adhes 29(8):785–795
15. Gunes R, Apalak MK, Yildirim M, Ozkes I (2010) Free vibration analysis of adhesively bonded single lap joints with wide and narrow functionally graded plates. Compos Struct 92(1):1–17
16. Parida SK, Pradhan AK (2014) 3d finite element analysis of stress distributions and strain energy release rates for adhesive bonded flat composite lap shear joints having pre-existing delaminations. J Mech Sci Technol 28(2):481–488
17. Kumar Y, Rammohan B, Budarapu PR, Harursampath DK, Seetharamu KN (2019) Dynamic instability analysis of multi-functional composite structures. AIAA J 57(10):4241–4254
18. Shetty H, Sethuram D, Rammohan B, Budarapu PR (2020) Low-velocity impact studies on GFRP and hybrid composite structures. Int J Adv Eng Sci Appl Math 12(3):125–141
19. Tewari K, Pandit MK, Budarapu PR, Natarajan S (2022) Analysis of sandwich structures with corrugated and spiderweb-inspired cores for aerospace applications. Thin-Walled Structures 180:109812
20. Farid G, Rachid B, Aurelian V (2022) Fatigue behavior of hybrid multi-bolted-bonded single-lap joints in woven composite plates. Int J Fatigue 58:106738
21. Budarapu PR, Thakur S, Kumar S, Paggi M (2021) Micromechanics of engineered interphases in nacre-like composite structures. Mech Adv Mater Struct 28(22):2327–2342
22. Budarapu PR, Kumar S, Khan MA, Rammohan B, Anitescu C (2022) Engineered interphase mechanics in single lap joints: analytical and PINN formulations. Int J Comput Methods. https://doi.org/10.1142/S0219876221430210
23. Dsouza SM, Varghese TM, Budarapu PR, Natarajan S (2020) A non-intrusive stochastic isogeometric analysis of functionally graded plates with material uncertainty. Axioms 9(3):92
24. Budarapu PR, Kumar S, Gangadhara Prusty B, Paggi M (2019) Stress transfer through the interphase in curved-fiber pullout tests of nanocomposites. Compos B Eng 165:417–434
25. Dusane AR, Budarapu PR, Pradhan AK, Natarajan S, Reinoso J, Paggi M (2021) Simulation of bridging mechanisms in complex

laminates using a hybrid PF-CZM method. Mech Adv Mater Struct, pp. 1–29
26. Pradhan AK, Parida SK (2013) 3d FE delamination induced damage analyses of adhesive bonded lap shear joints made with curved laminated FRP composite panels. J Adhes Sci Technol 27(10):1104–1121
27. Parida SK, Pradhan AK (2014) Influence of curvature geometry of laminated FRP composite panels on delamination damage in adhesively bonded lap shear joints. Int J Adhes Adhes 54:57–66
28. Kundu PK, Pradhan AK, Pandit MK (2020) Adhesion failure analysis in lap shear joint specimen subjected to transverse loading made of curved FGM. In: Advances in fluid mechanics and solid mechanics, Springer, pp 297–307
29. Koizumi MFGM (1997) FGM activities in japan. Compos B Eng 28(1–2):1–4